Materials Science & Engineering C 90 (2018) 308–313

Contents lists available at ScienceDirect

Materials Science & Engineering C

journal homepage: www.elsevier.com/locate/msec

Synthesis of monophasic Ag doped hydroxyapatite and evaluation of antibacterial activity

Madeeha Riaz[a,*], Rehana Zia[a], Ayesha Ijaz[a], Tousif Hussain[b], Munaza Mohsin[a], Abdul Malik[c]

[a] Physics Department, Lahore College for Women University, Lahore, Pakistan
[b] CASP, Government College University, Lahore, Pakistan
[c] National Institute of Lasers & Optronics (NILOP)/PIEAS, Islamabad, Pakistan

ARTICLE INFO

Keywords:
Biomaterials
Hydroxyapatite
Silver
Antibacterial activity

ABSTRACT

The present study aims to synthesized biomaterial that has antibacterial properties. Currently the surgical implants associated infections are a major cause of implant failure. Synthesis of silver doped hydroxyapatite as an antibacterial agent has potential importance to overcome post-surgical infections in a variety of clinical applications. Five silver doped hydroxyapatite $Ca_{10-x}Ag_x(PO_4)_6(OH)_2$ (x = 0, 0.1, 0.3, 0.5, 0.7 M) samples were synthesized by precipitation method and sintered at 900 °C to obtain well crystallized structure. No minor phase developed with silver addition, hexagonal hydroxyapatite (JCPDS# 09-432) was the single phase identified in all silver doped hydroxyapatite samples. The lattice parameter a and c changed with increase in silver concentration. The results of *in vitro* bioactivity revealed the bone bonding ability of silver doped hydroxyapatite samples. The antibacterial test showed that silver doped hydroxyapatite was sensitive to *Staphylococcus aureus* bacteria. Addition of silver significantly ($P < 0.005$) increased the antibacterial activity.

1. Introduction

Bioceramics is a new class of biomaterials that is used to replace damaged tissues and bones. These bioceramic materials have the ability of direct bonding with host bone tissues [1,2]. Synthetic hydroxyapatite ($Ca_{10}(PO_4)_6(OH)_2$) (HA) among these ceramics has been widely used for bone tissue engineering. Bones consist of 22% protein, 70% hydroxyapatite and 8% water. Natural bones are composed of hydroxyapatite nanoparticles having needle-like or rod-like shapes [3,4]. Chemical structure of HA is similar to human bone and it is widely used as coating for metal prosthesis, bone graft, drug [5] and antibiotics [6,7] carrier in bone-implant interface to reduce the bacterial infections. HA crystal is composed of OH^-, Ca^{2+} and PO_4^{-2} groups, which are closely packed in hexagonal arrangement and had space group of $P6_{3/m}$ with lattice parameter a = b = 9.423 A° and c = 6.875 A° [8]. Although, hydroxyapatite is the most osteoconductive and biocompatible material among other calcium phosphates, but it has limited antibacterial resistance [9]. Bacterial infections are the main cause of implant failure [10]. To overcome this problem Ag^+ is introduced to HA, since past silver has been recognized as strong inhibitor to bacterial growth [5]. Silver exhibits good thermal stability, low volatility, is biocompatible and non-toxic to human cell at low concentration along with superior antibacterial characteristics [11]. Previously, Ag^+ doped HA had been synthesized by several precipitation methods [12], microwave refluxing method [3], sol-gel method [13] ultrasonic precipitation method [14] electrostatic spray-pyrolysis process [6] and sintered at different temperatures from 800 to 1200 °C to obtain monophasic fully crystallized silver doped hydroxyapatite. When larger ionic radius (1.28 Å) Ag^+ is substituted to smaller ionic radius Ca^{+2} (0.99 Å) in hydroxyapatite lattice it provokes stress and strain in crystal structure [15]. These strains cause a stability problem in crystal structure. The theoretical limit of the Ag^+ substituting Ca^{+2} is 20% [16], but the practical limit is much lower than this. It is essential to optimize the concentration of dopant and sintering temperature to obtain monophasic hydroxyapatite, previous study show that < 3% concentration of silver [5,6] did not alter the crystalline structure of hydroxyapatite. The aim of the study is to use optimize temperature and dopant concentration to obtain monophasic hydroxyapatite structure. In the present study the inexpensive and conventional precipitation method has been selected to synthesize silver doped hydroxyapatite. To evaluate the antibacterial properties of HA by incorporating Ag^+ while maintaining bioactivity, and to demonstrate effects of Ag^+ concentration on crystallite size, crystallinity and lattice parameters.

* Corresponding author.
E-mail address: madeehariaz2762@yahoo.com (M. Riaz).

https://doi.org/10.1016/j.msec.2018.04.076
Received 18 August 2017; Received in revised form 16 March 2018; Accepted 25 April 2018
Available online 27 April 2018

2. Materials and methods

2.1. Synthesis of Ag doped HA

Precipitation method was used to synthesize silver-substituted hydroxyapatite nanoparticles expressed as follows (Eq. (1)):

$$(10 - x)Ca(NO_3)_2\Big)\cdot 4H_2O + xAgNO_3 + 6(NH_4)_2HPO_4 \xrightarrow[pH=10]{NH_4OH} Ca_{10-x}Ag_x(PO_4)_6(OH)_2$$
$$x = 0.0, 0.1, 0.3, 0.5 \text{ and } 0.7\ M \quad (1)$$

Silver nitrate ($AgNO_3$), calcium nitrate ($Ca(NO_3)_2\cdot 4H_2O$) and diammonium hydrogen phosphate ($(NH_4)_2HPO_4$) were used as the sources of Ag, Ca and P respectively. Ammonium hydroxide (NH_4OH) was used as a precursor to adjust the pH. Ag doped HA was synthesized by substituting Ca with Ag (x = 0.0, 0.1, 0.3, 0.5 and 0.7) while maintaining the molar ratio [Ca + Ag]:P to 1.67. Calcium and silver nitrate solution was prepared in 200 ml distilled water to obtain [Ca + (1 − x) Ag] (x = 0, 0.1, 0.3, 0.5, 0.7) molar solutions. Subsequently, 0.6 M phosphate solution prepared in distilled water was added drop wise to [Ca + (1 − x) Ag] solution under continuous stirring at 240 rpm and 50 °C temperature. The pH was maintained at 10 by adding ammonium hydroxide in the solution. The solution was continuously stirred for several hours until white precipitates of Ag doped HA were formed. These precipitates were then filtered and dried overnight at 100 °C. After drying the synthesized samples were sintered at 900 °C for 3 h. A schematic flowchart of precipitation method to synthesize Ag doped HA is as follows (Fig. 1).

2.2. Characterization

Five Ag doped HA samples were synthesized in this study. The X-ray Diffraction method (Bruker D8 Advance X-ray diffractometer using Cu Kα) was used to identify the crystalline phases developed after sintering. Phases were identified by matching the experimental XRD graphs to Joint Committee on Powder Diffraction Standards (JCPDS) files. Scherer's formula [16] was used to determine crystallite size of the samples and lattice parameter 'a' and 'c' was calculated by the formula: $\frac{1}{d^2} = \left[\frac{4}{3}(h^2 + k^2 + hk) + l^2\left(\frac{a^2}{c^2}\right)\right]\frac{1}{a^2}$. The functional group analysis was performed by Fourier transform Infrared spectroscopy (Midac M2000) recorded in 600 to 2400 cm^{-1} region. Raman spectroscopy (Advantage 532 Raman spectrometer) was performed to confirm the monophasic crystalline structure of samples as it is considered to be more sensitive to secondary phase as compared to XRD [15]. Raman spectra was recorded at 514 nm laser excitation wavelength. Bioactivity of the samples were examined by soaking the compacted samples in simulated body fluid [17] for one week incubated at 37 °C temperature under static condition.

Well diffusion method [18] was employed to determine the antibacterial activity of Ag doped HA against *Staphylococcus aureus* procured from the microbiology department of Post Graduate Medical Institute (PGMI), Lahore. The pure bacteria culture was first sub-cultured overnight in Nutrient broth (Merck, Germany) at 35 °C, then diluted 100 times in sterile water. The bacteria (~10^5 CFU) was inoculated on Nutrient agar (Merck, Germany) solidified on a sterilized petri dish and having four wells of 10 mm. For antibacterial test four different dilutions of each sample prepared in sterile distilled water, all measurements were performed in triplicate. One-way ANOVA test was performed to statistically analyze the antibacterial activity at $P < 0.05$ significance level.

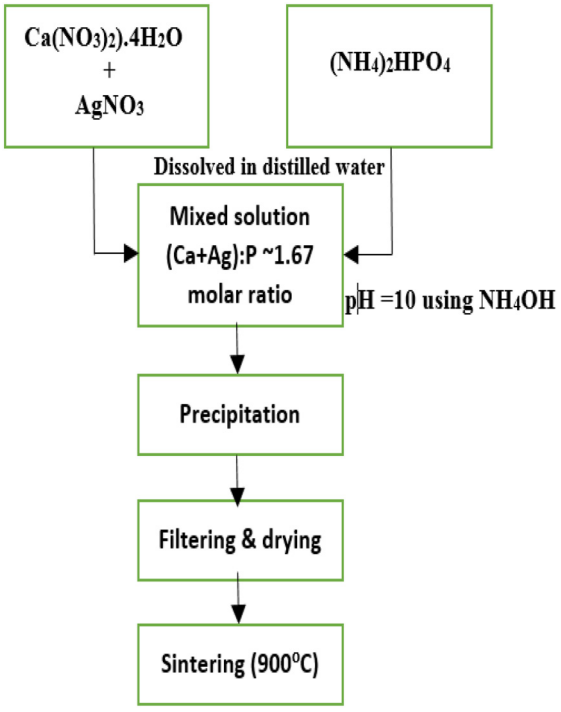

Fig. 1. Schematic flowchart of precipitation method.

3. Results and discussion

Fig. 2 demonstrates the X-ray Diffraction pattern of the silver doped hydroxyapatite samples sintered at 900 °C for 3 h. The peaks identified of (002), (102), (211), (300), (131), (222), (213), (004), (313), (034) and (520) reflections in all samples correspond to hexagonal hydroxyapatite crystalline phase (JCPDS#9-432). Absence of any secondary phase like CaO, Ag_3PO_4 or β-TCP indicates that silver ions have successfully substituted calcium ions without disturbing crystal lattice of hydroxyapatite. This result is in agreement with previous studies of Prekajsi et al. [19]. The diffraction peaks became sharp, well resolved and intensity increases with substitution of Ag^+ ions with Ca^{+2} ions indicating that hydroxyapatite phase developed is well crystallized and crystal growth increases with increase in Ag^+ content respectively. The peak reflections from (211), (300), (213) and (313) showed a slight peak shift. This may be attributed to changes in lattice parameter due to the smaller ionic radius of Ag^+ (1.28 Å) substituting Ca^{+2} (0.99 Å) or might be due to the presence of residual stresses and defect

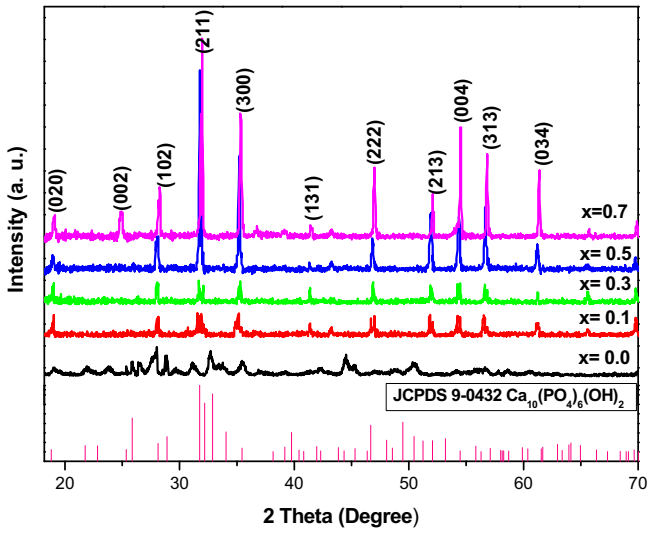

Fig. 2. XRD pattern of $Ca_{10-x}Ag_x(PO_4)_6(OH)_2$ sintered at 900 °C.

Table 1
Crystallite size, lattice parameter, volume of unit cell.

Sample	$Ca_{10-x}Ag_x(PO_4)_6(OH)_2$	Crystallite size (nm)	2 θ	hkl	Lattice parameter (A°)			Volume of cell
Name			Degree		a	c	c/a	
0AgHA	x = 0	21.5012	47.68	222	9.533	6.3551	0.666642	500.1491
0.1AgHA	x = 0.1	52.4452	47.66	222	9.537	6.3575	0.666614	500.7579
0.3AgHA	x = 0.3	66.8237	47.64	222	9.541	6.3607	0.66667	501.4303
0.5AgHA	x = 0.5	75.0575	47.64	222	9.546	6.3606	0.66631	501.9481
0.7AgHA	x = 0.7	83.4048	47.79	222	9.551	6.3621	0.666119	502.5926

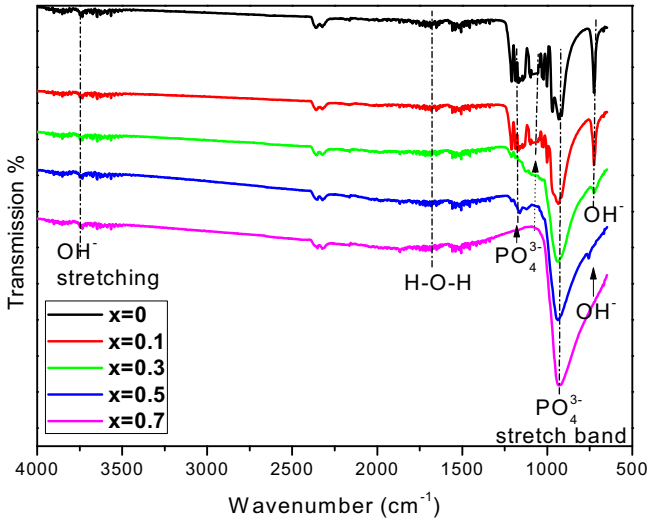

Fig. 3. FTIR pattern of $Ca_{10-x}Ag_x(PO_4)_6(OH)_2$ (x = 0, 0.1, 0.3, 0.5, 0.7).

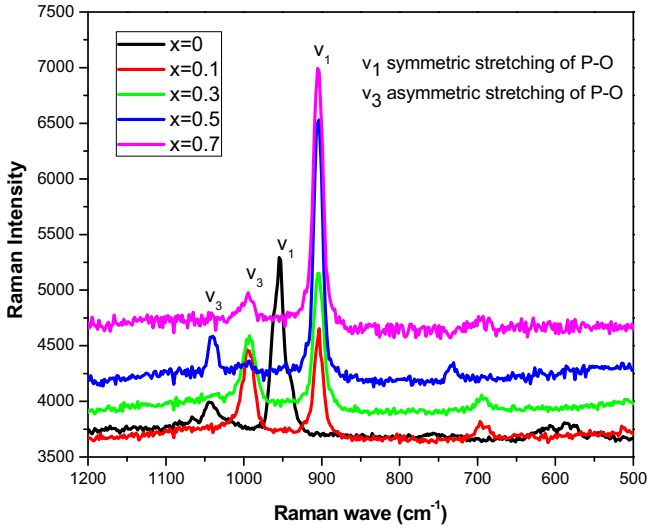

Fig. 4. Raman spectra of $Ca_{10-x}Ag_x(PO_4)_6(OH)_2$ (x = 0, 0.1, 0.3, 0.5, 0.7).

concentration, and sometimes due to misplacement of sample in X-ray instrument also result in shifting of peaks [20]. The average crystallite size (see Table 1) determined from (211), (300), (222) and (034) prominent peaks, increase in crystallite size was observed to increase in Ag^+ substitution. This increase in crystallite size results from an increase in nucleation site previously reported by Jadalannagari et al. [21].

An expansion of lattice parameter a and c (shown in Table 1) may cause due to substitution of larger ionic radius Ag^+ (0. 128 nm) to smaller ionic radius Ca^{+2} (0.099 nm) in hydroxyapatite crystal lattice. Previously it had been reported by Stanic et al. [7] that Ag^+ ion may not completely or partially replace Ca^{+2} ion it has the possibility to modify the crystalline environment as Ag^+ ion may occupy either lattice site or interstitial site depending on amount of Ag^+ incorporated [22]. The volume of the cell also expanded due to increase of lattice parameter. It was also observed that lattice parameter a and c increases with increase in Ag^+ concentration, however the c/a ratio remained constant. This result is in agreement with findings of Omer Kaygili et al. [23] that reported the change in lattice parameter is attributed to difference in ionic radius of Ag^+ substituting Ca^{+2} ions in the hydroxyapatite crystal lattice.

Fig. 3 shows FTIR spectra of silver doped hydroxyapatite samples sintered at 900 °C. FTIR spectra (Fig. 3) for all silver doped hydroxyapatite samples shows six bands corresponding to various vibrational modes originated from same or different functional groups (tabulated in Table 2). A sharp intense transmission band observed in FTIR spectra of 0AgHA at 921.51 cm^{-1} correspond to symmetric stretching mode of P–O in PO_4^{3-}. The same transmission band was observed at 932.45, 941.71, 943.39, 945.38 cm^{-1} for 0.1AgHA, 0.3AgHA, 0.5AgHA, 0.7AgHA samples respectively. Several other transmission bands (see Table 2 for detail) appeared in 1060–1161 cm^{-1} range was observed in all samples is attributed to the asymmetric stretching mode of PO_4^{3-}. Transmission bands appeared at 1687.44, 1685.39, 1695.61, 1692.54, 1692.52 cm^{-1} for 0.1AgHA, 0.3AgHA, 0.5AgHA, 0.7AgHA samples, respectively, attributed to bending mode of H-O-H, and same broad band observed at 3740.92 cm^{-1} for all samples is originated from hydroxyl group. No additional bands were observed, indicates that no impurity or secondary phase due to silver doping.

Raman spectra for silver doped hydroxyapatite samples are shown in Fig. 4 below. Raman spectroscopy is more sensitive against

Table 2
FTIR and Raman vibrational bands for silver doped hydroxyapatite.

FTIR bands (cm^{-1})					Raman bands (cm^{-1})					Band assignment
x = 0	x = 0.1	x = 0.3	x = 0.5	x = 0.7	x = 0	x = 0.1	x = 0.3	x = 0.5	x = 0.7	
724.58	724.58	725.05	756.21	–	–	–	–	–	–	Stretching mode of hydroxyl vibration
921.51	932.45	941.71	943.39	945.38	955.05	904.51	904.51	904.51	904.51	Symmetric stretching mode of P–O in PO_4^{3-}
1060.15	1073.43	1079.41	–	–	1044.01	993.46	992.53	1043.07	994.55	Asymmetric stretching of P–O in PO_4^{3-}
1144.95	1158.23	–	1161.74	–	–	–	–	–	–	Asymmetric stretching of P–O in PO_4^{3-}
1687.44	1685.39	1695.61	1692.54	1692.52	–	–	–	–	–	Bending mode of H–O–H in H_2O
3740.92	3740.92	3740.92	3740.92	3740.92	–	–	–	–	–	Symmetric stretching mode of the OH^-

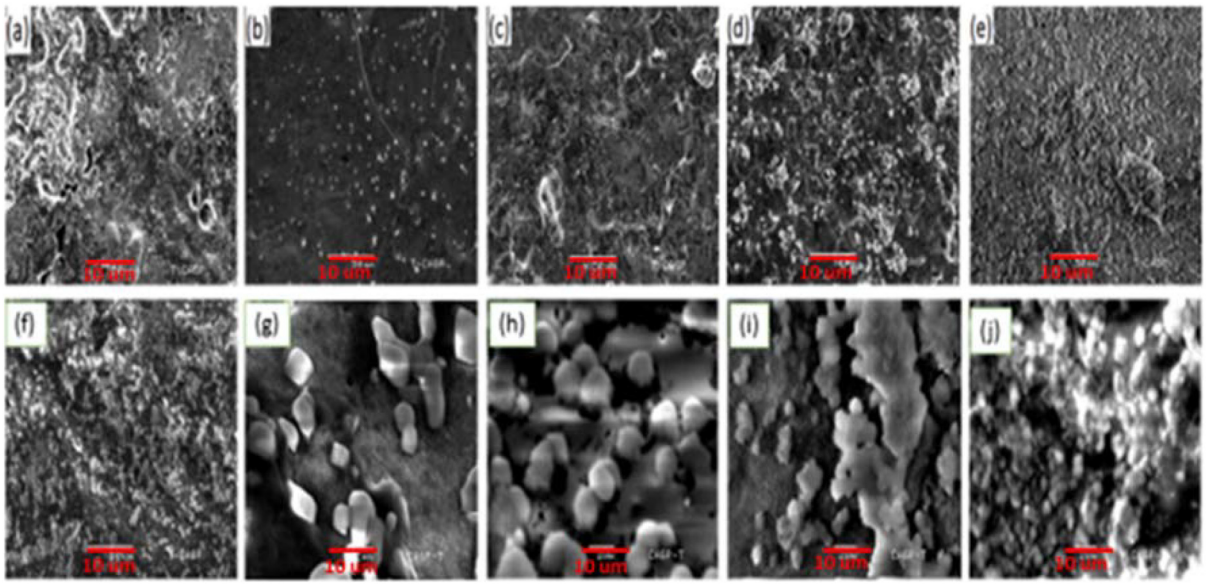

Fig. 5. SEM images of $Ca_{10-x}Ag_x(PO_4)_6(OH)_2$ (x = 0, 0.1, 0.3, 0.5, 0.7 from left to right) before (Fig (a), (b), (c), (d) and (e)) and after (Fig (f), (g), (h), (i) and (j)) immersion in SBF for 7 days.

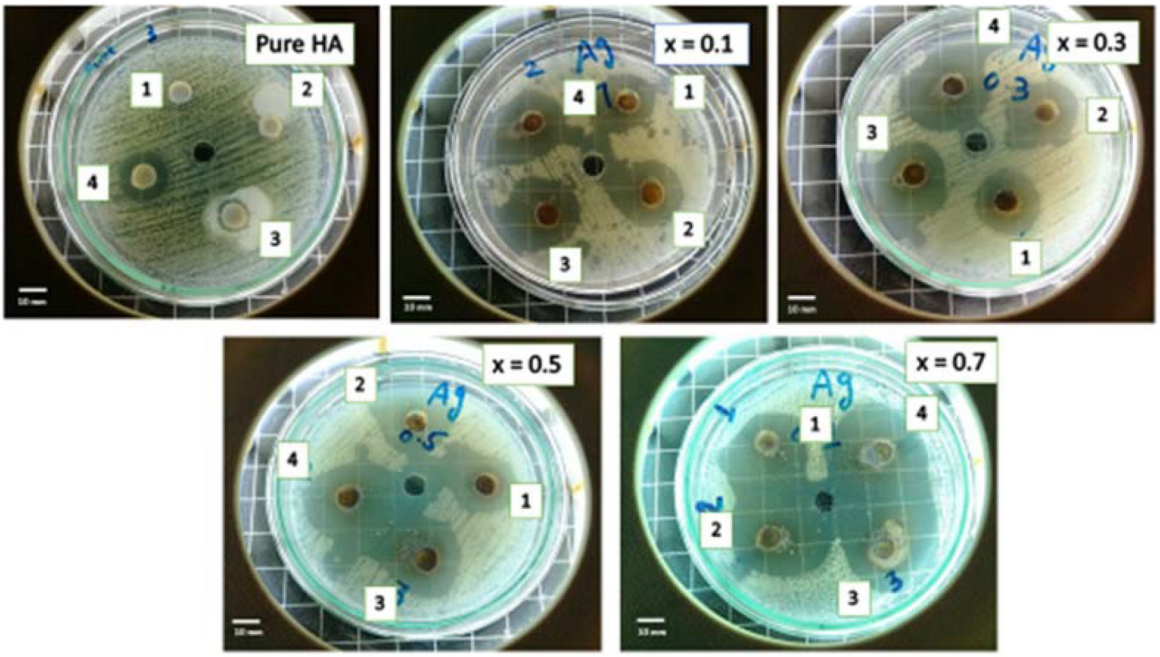

Fig. 6. Photographs of antibacterial test result of $Ca_{10-x}Ag_x(PO_4)_6(OH)_2$ (x = 0, 0.1, 0.3, 0.5, 0.7) against *Staphylococcus aureus* bacteria.

secondary phase as compared to other two techniques, *i.e.* XRD and FTIR [20]. Careful examination of Raman spectra revealed a strong band at 955.05 cm^{-1} for undoped sample corresponding to a symmetric stretching vibrational mode of PO_4^{3-} tetrahedral, same symmetric stretching band of PO_4^{3-} was observed at 904.51 cm^{-1} for all silver doped hydroxyapatite samples (0.1AgHA, 0.3AgHA, 0.5AgHA and 0.7AgHA). Other active band observed at 1044.01, 993.46, 992.53, 1043.07 and 994.55 cm^{-1} for 0AgHA, 0.1AgHA, 0.3AgHA, 0.5AgHA and 0.7AgHA sample respectively is attributed to asymmetric stretching of P—O. According to studies of Mishra et al. [20], Prekajski et al. [16] and Fowler [25] these characteristic stretching bands of PO_4^{3-} confirms the formation of hexagonal hydroxyapatite. According to previous studies [20,24], the presence of these characteristic vibrational bands of PO_4^{3-} and the hydroxyl group confirms the formation of pure hexagonal hydroxyapatite. Both FTIR and Raman spectroscopy results confirmed the formation of monophasic hydroxyapatite, and the absence of any secondary phase revealed that Ag^+ had successfully incorporated into the crystal lattice of hydroxyapatite without disturbing the crystal lattice.

Fig. 5(a, b, c, d and e) shows SEM images of 0AgHA, 0.1AgHA, 0.3AgHA, 0.5AgHA and 0.7AgHA respectively synthesized by precipitation method and sintered at 900 °C before soaking in simulated body fluid (SBF) [17], while Fig. 5(f, g, h, i and j) shows SEM images of 0AgHA, 0.1AgHA, 0.3AgHA, 0.5AgHA and 0.7AgHA respectively after immersion in SBF for 7 days at 37 °C. According to Kokubo [17] bioactivity or bone-bonding ability is often evaluated by the ability of any specimen to form an apatite layer on the surface in SBF. It is thought that this test is useful in predicting the *in vivo* bioactivity of specimen. The SEM images Fig. 5(f, g, h, i and j) after immersion in SBF reveals the formation of apatite crystals on the sample surface. With

Table 3
One-way ANOVA test: a statistical analysis of antibacterial activity against *Staphylococcus aureus*.

	Pair-wise mean comparison	Mean difference	Significance[a]
0.3 M	0.1AgHA 0AgHA	20	1
	0.3AgHA 0AgHA	24	1
	0.3AgHA 0.1AgHA	4	1
	0.5AgHA 0AgHA	25	1
	0.5AgHA 0.1AgHA	5	1
	0.5AgHA 0.3AgHA	1	1
	0.7AgHA 0AgHA	28	1
	0.7AgHA 0.1AgHA	8	1
	0.7AgHA 0.3AgHA	4	1
	0.7AgHA 0.5AgHA	3	1
0.7 M	0.1AgHA 0AgHA	25	1
	0.3AgHA 0AgHA	28	1
	0.3AgHA 0.1AgHA	3	1
	0.5AgHA 0AgHA	30	1
	0.5AgHA 0.1AgHA	5	1
	0.5AgHA 0.3AgHA	2	1
	0.7AgHA 0AgHA	34	1
	0.7AgHA 0.1AgHA	9	1
	0.7AgHA 0.3AgHA	6	1
	0.7AgHA 0.5AgHA	4	1
1.1 M	0.1AgHA 0AgHA	16	1
	0.3AgHA 0AgHA	19	1
	0.3AgHA 0.1AgHA	3	1
	0.5AgHA 0AgHA	21	1
	0.5AgHA 0.1AgHA	5	1
	0.5AgHA 0.3AgHA	2	1
	0.7AgHA 0AgHA	25	1
	0.7AgHA 0.1AgHA	9	1
	0.7AgHA 0.3AgHA	6	1
	0.7AgHA 0.5AgHA	4	1
1.5 M	0.1AgHA 0AgHA	14	1
	0.3AgHA 0AgHA	17	1
	0.3AgHA 0.1AgHA	3	1
	0.5AgHA 0AgHA	19	1
	0.5AgHA 0.1AgHA	5	1
	0.5AgHA 0.3AgHA	2	1
	0.7AgHA 0AgHA	20	1
	0.7AgHA 0.1AgHA	6	1
	0.7AgHA 0.3AgHA	3	1
	0.7AgHA 0.5AgHA	1	1

[a] Significance equal to 1 indicates that the means difference is significant and equal to 0 indicates that the means difference is not significant at the 0.05 level.

addition of Ag^+ more precipitation of apatite crystal was observed.

Fig. 6 shows the antibacterial activity test of Ag doped HA samples against gram positive bacteria *Staphylococcus aureus*. *Staphylococcus aureus* is considered to be one of the most common pathogenic organism that cause postsurgical wound infections. These infections are great risk because of their increasing frequency and high resistant behavior against antibiotic that ultimately result in failure of implant [10,26–28].

The antibacterial activity of samples was determined by measuring the diameter of the zone of inhibition. Four different dilutions 0.3 M, 0.7 M, 1.1 M and 1.5 M of each sample was prepared in 100 µl sterile distilled water. For undoped sample (0AgHA) no zone of inhibition was seen for low concentration 0.3 M and 0.7 M but for high concentration 1.1 M and 1.5 M the zone of inhibition was measured to be 11 ± 0.41 and 17 ± 0.51 mm respectively. Thus, undoped sample 0AgHA showed limited antibacterial activity. The antibacterial activity of hydroxyapatite (0AgHA) is attributed to either Ca^{+2} alkaline earth metal ions, Yuntao et al. [29] reported that Ca^{+2} ion is active membrane bactericide it destabilize cell membrane and kill stationary phase *Staphylococcus aureus,* or hydroxyl ions, according to findings of Siqueira et al. [30] hydroxyl ions are highly reactive oxidant free radicals that produce a lethal effect on bacterial cell, but both Ca and hydroxyl ions have limited antibacterial spectrum. The result (see Fig. 6) illustrates that the antibacterial activity significantly increased with increase in concentration of the Ag^+ doping agent. There was a bacterial inhibitory effect for all concentrations (0.3, 0.7, 1.1 and 1.5 M) of 0.1AgHA, 0.3AgHA, 0.5AgHA and 0.7AgHA silver doped HA samples. To determine the significance level of antibacterial activity for all samples one-way ANOVA statistical analysis (Table 3) was performed. $P < 0.05$ was selected level of significance for pair-wise mean comparison, it was found that all samples showed statistically significant antibacterial activity.

The 0.7AgHA sample showed the strongest antibacterial activity; measuring largest zone of inhibition. It can be assumed that release of Ag^+ ions from hydroxyapatite lattice is responsible for bactericidal effect. Silver is regarded as broad spectrum antibacterial agent [31–33]. N. Iqbal et al. [3] and Mocanu et al. [34] suggested that the Ag^+ ions interact with protein and enzymes of bacteria which result in structural damage of the cell membrane and death of bacterial cells, Ag^+ ion also disrupt the reproduction of bacteria it penetrates into the cell membrane bind itself to bacteria DNA and RNs and inhibits bacterial replication.

4. Conclusion

Monophasic silver doped hydroxyapatite was successfully synthesized by precipitation method and it was confirmed by XRD, FTIR and Raman spectroscopy. The analysis showed that a single phase of hexagonal hydroxyapatite was identified in all silver doped hydroxyapatite specimens with no minor phase, which indicates that Ag^+ was well substituted in lattice without disturbing the crystal structure. It was observed that 7% (0.7 M) of Ag^+ substituting in the Ca^{+2} site and sintering at 900 °C are the optimum limit to obtain monophasic hydroxyapatite crystalline structure. *In vitro* bioactivity test in SBF confirmed the bone-bonding ability of silver doped hydroxyapatite. The antibacterial assays showed that all silver doped hydroxyapatite samples had the bacteria inhibition ability and antibacterial activity increases significantly with increase in concentration of Ag^+. The undoped sample had limited antibacterial activity against *Staphylococcus aureus* while addition of Ag^+ enhanced antibacterial activity. From the present study it can be suggested that silver doped hydroxyapatite possessing antibacterial activity is a potentially good biomaterial for bone tissue engineering that can limit the risk of post-surgical infections caused by bacteria colonization.

References

[1] L.L. Hench, J. Wilson, Surface-active biomaterials, Science 226 (4675) (1984) 630–663.
[2] L.L. Hench, R.J. Splinter, W.C. Allen, T.K. Greenlee, Bonding mechanisms at the interface of ceramic prosthetic materials, J. Biomed. Mater. Res. 5 (6) (1971) 117–141.
[3] N. Iqbal, M.R.A. Kadir, N.H.B. Mahmood, S. Iqbal, D. Almasi, F. Naghizadeh, T. Kamarul, Characterization and biological evaluation of silver containing fluorapatite nanoparticles prepared through microwave synthesis, Ceram. Int. 41 (5) (2015) 6470–6477.
[4] J. Zhao, Z. Zhang, Z. Yu, Z. He, S. Yang, H. Jiang, Nucleation and characterization of hydroxyapatite on thioglycolic acid-capped reduced graphene oxide/silver nanoparticles in simplified simulated body fluid, Appl. Surf. Sci. 289 (2014) 89–96.
[5] N. Iqbal, A.R.M. Kadir, N.N.A.N. Malek, H.N. Mahmood, R.M. Murali, T. Kamarul, Rapid microwave assisted synthesis and characterization of nanosized silver-doped hydroxyapatite with antibacterial properties, Mater. Lett. 89 (2012) 118–122.
[6] K.S. Hwang, S. Hwangho, J.T. Kim, Silver-doped calcium phosphate nanopowders prepared by electrostatic spraying, J. Nanopart. Res. 10 (2008) 1337–1341.
[7] V. Stani'c, A.S. Radosavljevi'c-Mihajlovi'c, V. Zivkovi'c-Radovanovi'c, B. Nastasijevi'c, M. Marinovi'c-Cincovi'c, J.P. Markovi'c, M.D. Budimir, Synthesis, structural characterisation and antibacterial activityof Ag^+-doped fluorapatite nanomaterials prepared by neutralization method, Appl. Surf. Sci. 337 (2015) 72–80.
[8] D. Shi, Introduction to Biomaterials, 24(20) Tsinghua University Press, Beijing, 2006, pp. 3505–3510.
[9] M. Turkoz, O.A. Atilla, Z. Evis, Silver and fluoride doped hydroxyapatites: investigation by microstructure, mechanical and antibacterial properties, Ceram. Int. 39 (2013) 8925–8931.
[10] M. Riaz, R. Zia, F. Saleemi, H. Ikram, F. Bashir, In vitro antimicrobial activity of ZnO based glass–ceramics against pathogenic bacteria, J. Mater. Sci. Mater. Med. 268 (2015) 26.

[11] N. Rameshbabu, T.S. Sampath Kumar, T.G. Prabhakar, V.S. Sastry, K.V.G.K. Murty, K. Prasad Rao, Antibacterial nanosized silver substituted hydroxyapatite: synthesis and characterization, J. Biomed. Mater. Res. A 80 (3) (2007) 581–591.
[12] M. Turkoz, A.O. Atilla, Z. Evis, Silver and fluoride doped hydroxyapatite: investigation by microstructure, mechanical and antibacterial properties, Ceram. Int. 39 (2013) 8925–8931.
[13] Y. Yan, X. Zhang, Y. Huang, Q. Ding, X. Pang, Antibacterial and bioactivity of silver substituted hydroxyapatite/TiO_2 nanotube composite coatings on titanium, Appl. Surf. Sci. 314 (2014) 348–357.
[14] R.P. Singh, M. Singh, G. Verma, S. Shukla, Singh, S. Singh, Structural analysis of silver doped hydroxyapatite nanopowders by Rietveld refinement, Trans. Indian Inst. Metals 12-10 (2016) 1–8.
[15] M. Prekajski, B. Jokic, A. Kalijadis, J. Maletaškic, N. Stankovic, J. Lukovic, B. Matovic, Synthesis of silver doped hydroxyapatite nanospheres using Ouzo effect, Process. Appl. Ceram. 10 (2016) 169–174.
[16] R.D. Shannon, Revised effective ionic radii and systematic studies of interatomic distances in halides and chalcogenides, Acta Crystallogr. A 32 (1976) 751–767.
[17] T. Kokubo, H. Takadama, How useful is SBF in predicting in vivo bone bioactivity? Biomaterials 27 (2006) 2907–2915.
[18] M. Balouiri, M. Sadiki, S.K. Ibnsouda, Methods for in vitro evaluating antimicrobial activity: a review, J. Pharm. Anal. 6 (2016) 71–79.
[19] M. Riaz, R. Zia, F. Saleemi, T. Hussain, F. Bashir, H. Ikhram, Effect of Ti^{+4} on in vitro bioactivity and antibacterial activity of silicate glass-ceramics, Mater. Sci. Eng. C 69 (2016) 1058–1067.
[20] K.V. Mishra, B.S. Rai, P.B. Asthana, O. Parkash, D. Kumar, Effect of annealing on nanoparticles of hydroxyapatite synthesized via microwave irradiation: structural and spectroscopic studies, Ceram. Int. 40 (2014) 11319–11328.
[21] S. Jadalannagari, K. Deshmukh, S.R. Ramanan, M. Kowshik, Antimicrobial activity of hemocompatible silver doped hydroxyapatite nanoparticles synthesized by modified sol–gel technique, Appl. Nanosci. 4 (2) (2014) 133–141.
[22] R. Zamiri, K.B. Singh, D. Dutta, A. Reblo, F.M.J. Ferreira, Electrical properties of Ag-doped ZnO nano-plates synthesized via wet chemical precipitation method, Ceram. Int. 40 (2014) 4471–4477.
[23] O. Kaygili, S. Keser, V.S. Dorozhkin, F. Yakuphanoglu, A.A. Al-Ghamdi, S. Kirbag, D. Sertkaya, T. Atles, C.N. Gursoy, Structural and dielectrical properties of Ag- and Ba-substituted hydroxyapatites, J. Inorg. Organomet. Polym. 24 (2014) 1001–1008.
[24] R. Zia, M. Riaz, S. Maqsood, S. Anjum, Z. Kayani, T. Hussain, Titania doped bioactive ceramics prepared by solid state sintering method, Ceram. Int. 41 (2015) 8964–8972.
[25] O.B. Fowler, Infrared studies of apatites. I. Vibrational assignments for calcium, strontium, and barium hydroxyapatites utilizing isotopic substitution, Inorg. Chem. 13 (1) (1974) 194–207.
[26] W. CisTs, M.D. HowE, The problem of postoperative wound infections caused by *Staphylococcus aureus*, Ann. Surg. 146 (3) (1957) 384–396.
[27] M. Razavi, S.D. Shepard, A.J. Suaya, B.W. Stason, Postoperative *Staphylococcus aureus* infections in Medicare beneficiaries, PLoS One 9 (11) (2014) e110133.
[28] C.Y.S. Tong, Joshua S. Davis, Emily Eichenberger, Thomas L. Holland, Vance G. Fowler Jr., *Staphylococcus aureus* infections: epidemiology, pathophysiology, clinical manifestations, and management, Clin. Microbiol. Rev. 28 (3) (2015) 603–6611.
[29] Yuntao Xie, Lihua Yang, Calcium and magnesium ions are membrane-active against stationary-phase *Staphylococcus aureus* with high specificity, Sci. Rep. 6 (2016) 20628.
[30] J.F. Siqueira Jr., H.P. Lopes, Mechanisms of antimicrobial activity of calcium hydroxide: a critical review, Int. Endod. J. 32 (5) (1999) 361–369.
[31] M.J. Hajipour, K.M. Fromm, A.A. Ashkarran, D.J. de Aberasturi, I.R. de Larramendi, T. Rojo, V. Serpooshan, W.J. Parak, M. Mahmoudi, Antibacterial properties of nanoparticles, Trends Biotechnol. 30 (10) (2012) 499–511.
[32] S.C. Ciobanu, L.S. Iconaru, C.M. Chifiriuc, A. Costescu, L.P. Coustumer, Daniela Predoi, Synthesis and antimicrobial activity of silver-doped hydroxyapatite nanoparticles, Biomed. Res. Int. 2013 (2013) 1–10 (91621810).
[33] S.C. Ciobanu, F. Florian Massuyeau, V.L. Constantin, D. Predoi, Structural and physical properties of antibacterial Ag-doped nano-hydroxyapatite synthesized at 100 °C, Nanoscale Res. Lett. 6 (2011) 613.
[34] A. Mocanu, G. Furtos, S. Rapuntean, O. Horovitz, C. Flore, C. Garbo, M. Tomoaia-Cotisel, Synthesis; characterization and antimicrobial effects of composites based on multi-substituted hydroxyapatite and silver nanoparticles, Appl. Surf. Sci. 298 (2014) 225–235.